

Provided for non-commercial research and educational use only.  
Not for reproduction or distribution or commercial use.



This article was originally published in a journal published by Elsevier, and the attached copy is provided by Elsevier for the author's benefit and for the benefit of the author's institution, for non-commercial research and educational use including without limitation use in instruction at your institution, sending it to specific colleagues that you know, and providing a copy to your institution's administrator.

All other uses, reproduction and distribution, including without limitation commercial reprints, selling or licensing copies or access, or posting on open internet sites, your personal or institution's website or repository, are prohibited. For exceptions, permission may be sought for such use through Elsevier's permissions site at:

<http://www.elsevier.com/locate/permissionusematerial>

# Multifocal two-photon laser scanning microscopy combined with photo-activatable GFP for *in vivo* monitoring of intracellular protein dynamics in real time

Joerg Martini <sup>a,1</sup>, Katja Schmied <sup>b,1</sup>, Ralf Palmisano <sup>b</sup>, Katja Toensing <sup>a</sup>,  
Dario Anselmetti <sup>a,\*</sup>, Thomas Merkle <sup>b</sup>

<sup>a</sup> Department of Experimental Biophysics and Applied Nanoscience, Faculty of Physics, University of Bielefeld, 33615 Bielefeld, Germany

<sup>b</sup> Department of Genomic Research, Faculty of Biology, University of Bielefeld, 33594 Bielefeld, Germany

Received 11 August 2006; received in revised form 20 December 2006; accepted 21 December 2006

Available online 17 January 2007

## Abstract

We used multifocal two-photon laser scanning microscopy for local and selective protein activation and quantitative investigation of intracellular protein dynamics. The localized activation was realized with photo-activatable green-fluorescent-proteins (pa-GFP) and optical two-photon excitation in order to investigate the real-time intracellular dynamics *in vivo*. Such processes are of crucial importance for a deep understanding and modelling of regulatory and metabolic processes in living cells. Exemplarily, the intracellular dynamics of the Arabidopsis MYB transcription factor LHY/CCA1-like 1 (LCL1) that contains both a nuclear import and a nuclear export signal was quantitatively investigated. We used tobacco BY-2 protoplasts co-transfected with plasmids encoding photo-activatable green fluorescent protein (pa-GFP) fusion proteins and a red fluorescing transfection marker and measured the rapid nuclear export of pa-GFP-LCL1 after its photo-activation in the nucleus. In contrast, an export-negative mutant of LCL1 remained trapped inside the nucleus. We determined average time constants of 51 s and 125 s for the decrease of fluorescence in the nucleus due to active bi-directional nuclear transport of pa-GFP-LCL1 and diffusion of pa-GFP, respectively.

© 2007 Elsevier Inc. All rights reserved.

**Keywords:** Multifocal multiphoton laser scanning microscopy; pa-GFP; Protein dynamics; DsRed

## 1. Introduction

Conventional laser scanning microscopy reveals only a quasi-stationary glimpse of protein dynamics at a given steady state. The investigation and quantitative real-time analysis of intracellular protein dynamics therefore requires the combination of a fast microscopy technique with high spatial and temporal resolution and the ability for locally confined and selective labelling. Both criteria are met by combination of 2-photon (2P)-activation of photo-activatable green-fluorescent protein (pa-GFP; Post et al., 2005) fusion proteins and conventional fluorescence microscopy,

1-photon laser scanning microscopy (1PLSM) or 2-photon laser scanning microscopy (2PLSM) for detection of labelled fluorophores. The volume of pa-GFP activation can be precisely and restrictively confined to a defined region within the cell by 2P-activation, limited by the diffraction limit of laser focussing. Selective detection of pa-GFP implies spectral activation at  $\lambda \sim 408$  nm, which induces a photoconversion resulting in a shift of the absorption maximum of the fluorescent protein to  $\lambda \sim 504$  nm with a maximum of emission at  $\lambda \sim 517$  nm (Patterson and Lippincott-Schwartz, 2002; Patterson and Lippincott-Schwartz, 2004).

The method of 2P-activation of pa-GFP combines several advantages that ensure cell viability, local and selective excitation of fluorescent probes by a 2-photon process keeping photobleaching and cell damage at very low levels

\* Corresponding author. Fax: +49 521 106 2959.

E-mail address: [dario.anselmetti@physik.uni-bielefeld.de](mailto:dario.anselmetti@physik.uni-bielefeld.de) (D. Anselmetti).

<sup>1</sup> These authors contributed equally to this work.

(König, 2000). The intrinsic limitation of excitation to the microscope's focal plane, provided by the axial sectioning capability of 2PLSM (Denk et al., 1990; Diaspro, 2002), is also responsible for the spatial confinement and selectivity of the 2P-activation of pa-GFP. Only those molecules in the focus (activated by a burst of femtosecond 720–840 nm laser light pulses) will be photo-activated and hence will emit fluorescence at  $\lambda \sim 520$  nm when excited with light of  $\lambda \sim 488$  nm by 1PLSM or  $\lambda > 920$  nm by 2PLSM, respectively (Schneider et al., 2005). The use of near-infrared laser light for activation and detection is reasoned by the specific cross sections of pa-GFP, but it also provides the advantage of a higher penetration depth, negligible one-photon cross sections, and less potential for cellular damage and fluorescent background (Zipfel et al., 2003a; Zipfel et al., 2003b).

Nucleo-cytoplasmic partitioning of proteins such as transcription factors offers a fast and reversible tool to regulate gene expression, for instance upon extra-cellular and intra-cellular signals (Merkle, 2003). Regulated nucleo-cytoplasmic partitioning of transcription factors is just one example of fast protein dynamics that exist in a living cell and that are crucial for signal transduction and cell homeostasis. Monitoring protein movements in living cells is therefore of key interest for the quantitative understanding of the spatio-temporal dynamics of regulatory networks involving protein interaction. The Arabidopsis transcription factor LCL1 (LHY/CCA1-like 1) is a member of the MYB1R family with high similarity to the MYB domains of Arabidopsis clock proteins (Schaffer et al., 1998; Wang and Tobin, 1998). LCL1 contains both a nuclear localisation signal (NLS) and a nuclear export signal (NES) and

therefore is an actively translocating nucleo-cytoplasmic shuttle protein. In contrast, the localisation of the small protein pa-GFP alone is distributed within the cell by diffusion, only. We used transient expression of pa-GFP-LCL1 fusion proteins in tobacco BY-2 protoplasts and multifocal 2PLSM to monitor nucleo-cytoplasmic dynamics of this transcription factor *in vivo*. Co-transfection with red-fluorescent protein (DsRed)-tagged prenylated Rab acceptor 1 (Pra1; At2g38360), a membrane-localised protein that localises in speckles around the nuclear envelope, is necessary for identification and visualisation of transfected protoplasts before activation. Upon combining pa-GFP and multifocal 2PLSM, we demonstrate that real-time imaging of dynamics of pa-GFP fusion proteins can directly be used with high spatial and temporal resolution under *in vivo* conditions.

## 2. Materials and methods

### 2.1. Parallelized 64 foci two-photon laser scanning microscopy

Pa-GFP-activation and fluorescence detection *in vivo* was realised by multifocal 2PLSM, based on a commercial system (TriM-Scope, LaVision-Biotec; Martini et al., 2005; Nielsen et al., 2001) that was modified according to the specific needs of dynamic protein monitoring (Fig. 1). The 64 foci 2PLSM (Martini et al., 2006) is a combination of an inverted optical microscope (IX 71, Olympus) and of a mode-locked femtosecond Ti:Sa laser pumped by a solid-state laser (Tsunami & Millennia X, both Spectra Physics) generating 100 fs laser pulses between 760 nm and 960 nm.

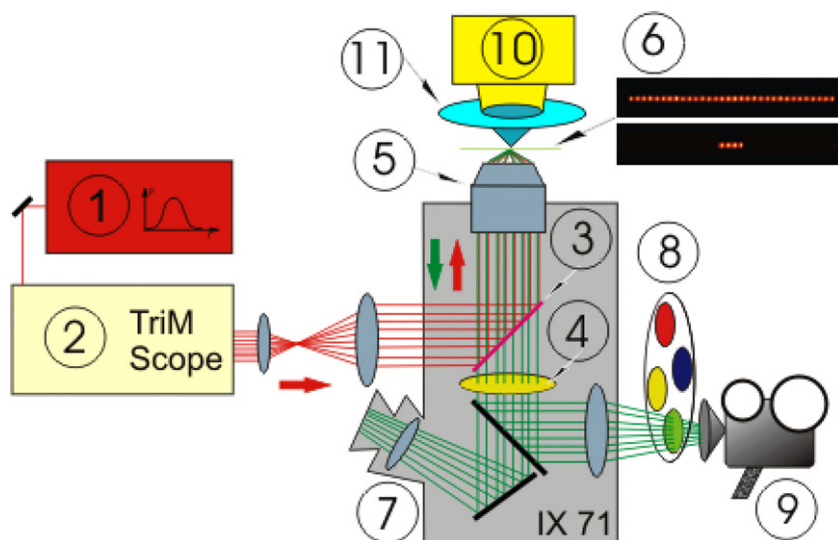


Fig. 1. Schematic setup of the multifocal 2-photon laser scanning microscope. (1) Tsunami Ti:Sa laser (wavelength adjustable) pumped by solid state Millennia X laser (both Spectra Physics), (2) multifocal laser scanning unit (TriM-scope, LaVision BioTec), (3) dichroic mirror (2P-Beamsplitter, Chroma), (4) short pass filter (2P-Emitter, Chroma), (5) objective lens (UPLAO60XW3/IR, NA = 1.2; Olympus), (6) selectable number of fluorescence inducing foci in the sample, (7) inverted optical microscope (IX 71, Olympus), (8) filter wheel (filter wheel, LaVision BioTec) equipped with bandpass emission filters D 605/55 (Chroma) for Ds-Red and HQ525/50 in combination with HQ510/20 (both Chroma) for pa-GFP, (9) back illuminated EMCCD-camera (IXON DV887ECS-UVB, Andor Technology) in non-descanned detection path, (10) fluorescence lamp (HBO 50, Zeiss), (11) bandpass excitation filter D 540/25 (Chroma) for Ds-Red or bandpass excitation filter HQ 480/20 (Chroma) for pa-GFP. Further are described in the text.

Selection of wavelengths for activation and imaging cycles is performed using a home-built screw motorization that allows wavelength tuning within 5 s. The laser scanning unit (TriM-Scope, LaVision-BioTec) consists of an internal pre-chirp section that compensates for laser pulse dispersion, a beam multiplexing section and two galvanometric mirror scanners. Via a set of ten 100% reflective mirrors and one adjustable 50% mirror the exciting NIR laser beam is split up in 1, 2, 4, ..., 64 exciting foci in the sample. This adjustable number of foci is scanned in the focal plane of the microscope's objective lens (UPLAO60XW3/IR, NA = 1.2; Olympus) by the two scanning mirrors inside the laser scanning unit. All activation and measurement procedures were performed in a temperature-controlled environment at  $293 \pm 1$  K.

As the multiple foci generate a relatively high two photon-induced fluorescence yield while keeping the energy deposition in each individual focus under the sample's deterioration limit, imaging is possible with 30 ms time resolution. Images are taken by a back-illuminated EMCCD camera (IXON DV887ECS-UVB, Andor Technology) in a non-descanned manner. The exciting NIR laser beams are directed via a dichroic mirror (2P-Beamsplitter, Chroma) onto the back aperture of the objective lens while NIR stray light in the detection path is blocked by a short pass filter (2P-Emitter, Chroma). To allow for depth and spectral fluorescence sectioning, the inverted microscope is equipped with a mechanical focus drive (MFD, Märzhäuser) and a programmable filter wheel (LaVision-BioTec). Data acquisition and experiment control is performed by TriM-Scope's software package Imspector (LaVision-BioTec). Handling and processing of the 5-dimensional fluorescent data sets, including spectral and temporal data axis, is either realised with software packages Imspector (LaVision-BioTec), ImageJ (Rasband, 1997) or Imaris (Bitplane).

## 2.2. Generation of plasmids and transient transfection of tobacco BY-2 protoplasts

The cDNA encoding pa-GFP (a generous gift from J. Lippincott-Schwartz) was amplified by PCR using primers that added a 5' *Xba*I site just before the start codon and a 3' *Eco*RI site just after the last codon. The stop codon of the pa-GFP cDNA was omitted in order to be able to create in-frame fusions 3' to pa-GFP. The resulting DNA fragment was restriction digested with *Xba*I and *Eco*RI and ligated into the plasmid p5'GFP (Haasen et al., 1999) that had been digested with the same restriction enzymes. In this way, the cDNA encoding GFP(S65T) in the plasmid p5'GFP was replaced by the cDNA encoding pa-GFP, resulting in plasmid p5'paGFP. This plasmid consisting of the strong constitutive 35S promoter of cauliflower mosaic virus that drives the expression of pa-GFP and the nopalinsynthase terminator in the pUC19 backbone was used to transfect tobacco BY-2 protoplasts using the polyethylene glycol method as described (Haasen et al., 1999). Plasmids

encoding pa-GFP-LCL1 and pa-GFP-LCL1(NESm) were generated by ligation of the LCL1 or LCL1(NESm) cDNA, respectively, into the *Eco*RI and *Xho*I sites of p5'paGFP. In the same way, plasmids encoding GFP-LCL1 and GFP-LCL1(NESm) were generated using plasmid p5'GFP (Schmied and Merkle, submitted for publication). The plasmid encoding GFP-NLS-CHS-NESm (referred to as GFP-NLS) was described previously (Haasen et al., 1999). The transfection marker Pra1-DsRed (At2g38360-DsRed) was generated by inserting the At2g38360 cDNA fused in-frame to DsRed (Clontech) into the *Bam*HI and *Sac*I sites of p3'GFP (Haasen et al., 1999). For double transfections, 20  $\mu$ g of each plasmid was used. All cDNA fragments created by PCR were sequenced to confirm their integrity.

## 2.3. Statistics

Average fluorescence intensity data sets in the nucleus were generated with the ImageJ "ZProfiler" plugin by choosing the nucleus area as region of interest in the original 16-bit camera image time series. Mono- and bi-exponential fitting (Levenberg-Marquardt algorithm) of these data sets were then applied to the fluorescence decrease regime utilising Origin 6.0 (Microcal). Fit iterations were carried out until fit parameters did not change with following iterations. For statistical analysis only those fits that showed  $R^2 > 0.95$  for pa-GFP-LCL1 and  $R^2 > 0.94$  for pa-GFP were taken into account. For pa-GFP-LCL1 standard deviation of individual fits remained  $< 10.6$  s and for pa-GFP  $< 5.26$  s. In both cases, data from seven independent experiments met the statistical criteria for being considered.

## 3. Results

### 3.1. Analysis of nucleo-cytoplasmic partitioning of a transcription factor

Transient transfection assays employing reporter genes encoding fluorescent proteins have proven to be valuable fast and non-invasive tools for *in vivo* analyses of cellular processes, including protein activity and localisation. This is demonstrated by the analysis of the nucleo-cytoplasmic partitioning of the Arabidopsis MYB transcription factor LCL1 (At5g02840) in plant protoplasts. The fusion protein consisting of GFP and wild-type LCL1 localises to the nucleus and to the cytoplasm (Fig. 2a). The partitioning of GFP-LCL1 between these two cellular compartments was dramatically shifted towards an almost nuclear localisation after incubation of the protoplasts with the nuclear export inhibitor leptomycin B (LMB; Fig. 2b). LMB covalently modifies the nuclear export receptor XPO1 (in humans designated CRM1; Fornerod et al., 1997; Fukuda et al., 1997) thus specifically inhibiting nuclear export of cargo macromolecules that bind to this nuclear transport receptor (Kudo et al., 1999). The LMB-sensitive nucleo-cytoplasmic partitioning of the transcription factor LCL1 therefore clearly indicates the presence of a nuclear export signal

(NES) for XPO1-dependent nuclear transport. In contrast, the localisation of GFP alone was not affected by LMB at all (Figs. 2c and d). On the other hand, mutation of the NES in LCL1 (Schmied and Merkle, submitted for publication) resulted in nuclear accumulation of the GFP fusion protein due to the presence of a classic basic nuclear import signal (NLS; Figs. 2e and f). The steady state localisation of LCL1 (Fig. 2a) is thus a function of the balance between nuclear export and re-import.

While 1PLSM analysis of the localisation of GFP fusion proteins reveals their steady state localisation, the availability of pa-GFP (Post et al., 2005) combined with localised 2P photo-activation offers the possibility to analyse the dynamics that form the basis of the localisation of proteins at equilibrium. The efficiencies of transient transfection procedures of plant protoplasts and plant cells are generally rather low. Since pa-GFP cannot be detected easily before its photo-activation, we established a co-transfection protocol with a fluorescent marker that enabled us to quickly identify transfected among many non-transfected protoplasts. We chose *At2g38360* fused to DsRed as a fluorescent co-transfection marker. This gene encodes an Arabidopsis protein with high similarity to prenylated Rab acceptor (Pra1; Hutt et al., 2000). The fusion protein localises to membranes of the endoplasmic reticulum and/or Golgi (Merkle, unpublished). The red fluorescence is detected in discrete foci in the cytoplasm that do not interfere with pa-GFP fusion protein analysis and often surround and thereby mark the position of the cell nucleus (Figs. 2g and h).

### 3.2. Selective and localised activation of pa-GFP in the nucleus

In non-linear microscopy multiple-photon excitation processes strongly depend on spatial and temporal confinement of photons due to the extremely low cross section for multiple-photon excitation (Albota et al., 1998; Cahalan et al., 2002). Unlike with 1P excitation processes, this characteristic feature allows very selective and locally confined activation of pa-GFP in the focal volume by femtosecond laser pulses delivering the necessary energy densities (here: 100 fs, 800 nm, 30–70 mW, 4–8 foci). Positioning such laser foci in the cell nucleus allows selective limitation of pa-GFP photo-activation within the focal volume given by the numerical aperture of the objective lens, the refraction index and the laser wavelength. In our experiment the depth of our focal volume and therefore the length scale of 2P-activation is approximately 1  $\mu\text{m}$ , corresponding to a volume in the femtoliter range. This is considerably smaller than the average diameter of a typical plant nucleus, like those of tobacco BY-2 cells (Figs. 2e and f).

### 3.3. Real-time fluorescence imaging of protein dynamics

After selective pa-GFP activation, fluorescence imaging of cellular protein dynamics was realised by either of two

working procedures that differ from each other by an operational point of view. The first procedure is based on standard 1P fluorescence imaging of pa-GFP (with emission filters: HQ525/50 and HQ510/20) that allows real-time transmission fluorescence observation of pa-GFP dynamics at the same time as its 2P activation. The second procedure is based on 2P fluorescence imaging of pa-GFP with femtosecond laser pulses now tuned to the new pa-GFP absorption wavelength of 920 nm after its photo-activation at 800 nm. Since this wavelength tuning inevitably produces an observation time gap of about 5 s, both procedures have been used to gain full temporal and spatial information about fluorescent protein dynamics.

### 3.4. Activation and protein dynamics of pa-GFP

First, we recorded the 2P-activation of pa-GFP in the nucleus and the dynamics of its diffusion within the BY-2 protoplast. A selection of five images out of a whole series of 1P-transmission-fluorescence images are shown (Fig. 3), consecutively taken at the start of recording before photo-activation (0 s), at the start of photo-activation (26 s), and at 33 s, 180 s and 1000 s after start of recording. The cell nucleus is indicated by a red ellipse that has been selected as a region of interest (ROI) for the subsequent determination of the fluorescence intensity. The decrease of fluorescence intensity over time as seen in the last four images directly displays the diffusion of pa-GFP into the cytoplasm. Paralleled by the decrease of nuclear fluorescence, an increase of the fluorescence in the cytoplasm can clearly be detected. It is noteworthy that the rectangular shape of the strong fluorescence signal at time point 26 s (Fig. 3b) reflects the fact that pa-GFP activation was accomplished by scanning 4 fs-laser foci for 3 s in the activation area of  $7 \times 8 \mu\text{m}^2$  within the nucleus, rather than by single point activation, only.

In order to quantify the kinetics of the decrease of pa-GFP fluorescence in the nucleus, we analysed the fluorescence intensity within the chosen ROI over the whole series of fluorescence images (Fig. 4). The onset of the 1P-fluorescence intensity curve is dominated by a sharp peak at 26–29 s after the start of recording, reflecting the photo-switching of pa-GFP by the 3-s laser burst at 800 nm. Directly after pa-GFP activation (about 29 s after the start of recording), the averaged fluorescence intensity is about 5 times greater as compared to the pre-activation intensity. Afterwards, a decrease of nuclear fluorescence intensity in time was recorded which is due to the diffusion of activated pa-GFP fluorophores out of the nucleus into the cytoplasm (compare Figs. 3c and d). Later on, also photobleaching becomes noticeable as can be deduced from the over all reduction in fluorescence intensity in the entire cell (compare Figs. 3d and e). This interpretation is supported by the fact that the decrease of nuclear fluorescence over time cannot be explained properly by a single exponential function. However, bi-exponential fitting describes the observed decrease in excellent approximation (Fig. 4, red line). With this fit, time constants for the two processes after pa-GFP

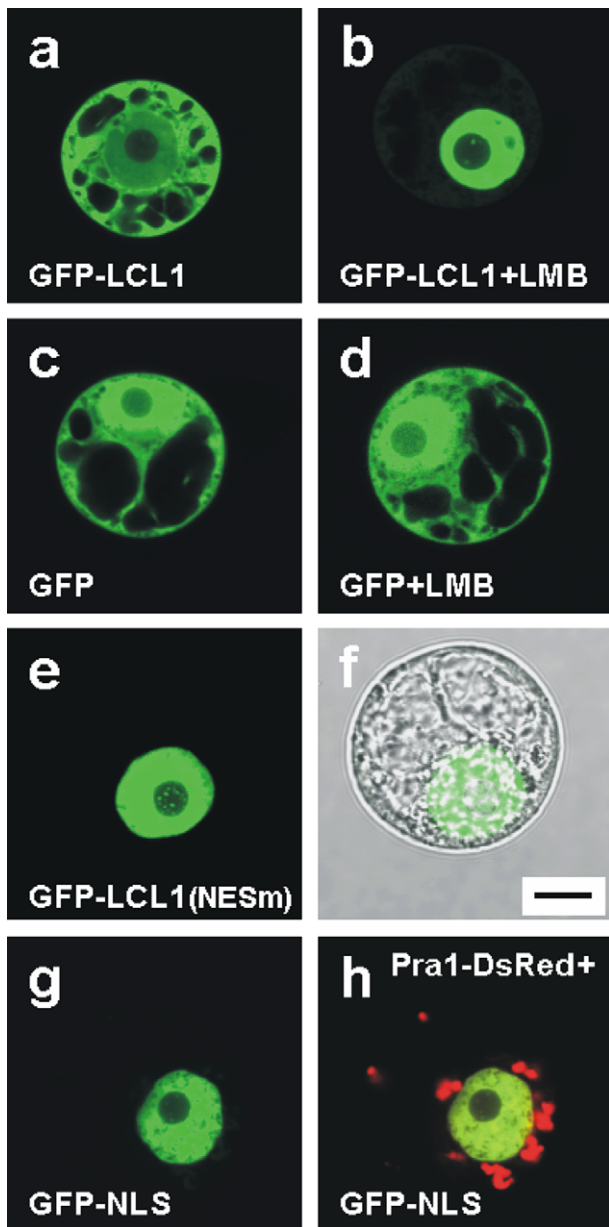


Fig. 2. The Arabidopsis transcription factor LCL1 contains a nuclear import and a nuclear export signal (NLS, NES, respectively). Tobacco BY-2 protoplasts were transfected with plasmids encoding GFP fusion proteins as indicated. The steady state localisation of these GFP fusion proteins was analysed by IP confocal laser scanning microscopy. (a) GFP-LCL1 reveals partitioning between the nucleus and the cytoplasm. (b) The steady state partitioning of GFP-LCL1 is shifted dramatically towards an almost complete nuclear localisation after incubation with the nuclear export inhibitor leptomycin B (LMB), due to the presence of a functional NLS. (c,d) In contrast, LMB has no effect on the localisation of GFP alone. (e) Elimination of the nuclear export activity of LCL1 by point mutation of its NES in GFP-LCL1(NESm) also results in nuclear accumulation of the GFP fusion protein. (f) Overlay of the transmission and the GFP fluorescence image of the same protoplast shown in (e). The scale bar represents 10  $\mu\text{m}$ . (g) Accumulation of GFP-NLS in the nucleus as control. (h) Overlay of the green fluorescence of GFP-NLS and the red fluorescence of Pra1-DsRed (At2g38360) that was used as a transfection marker in the same protoplast.

photo-activation in the nucleus could be calculated, resulting in 175 s for pa-GFP diffusion and in 2100 s for photobleaching (Fig. 4). In order to determine the three dimensional distribution within the BY-2 protoplast, we analysed the DsRed and pa-GFP fluorescence by 2PLSM. This imaging was performed using the fast parallel 64 foci mode of our TriM-Scope that allows sensitive optical sectioning with respect to spectral emission characteristics by using appropriate emission filters. As result, the 2P-fluorescence voxel representations are shown, where the DsRed-tagged At2g38360 and pa-GFP are coloured in red and green, respectively (Figs. 5a and b). Whereas the transfected protoplast before photo-activation only exhibits the red fluorescence of the transfection marker At2g38360-DsRed (Fig. 5a), the pa-GFP fluorophores that had been activated in the nucleus clearly diffused into the cytoplasm, as shown in the image taken 400 s after start of recording (Fig. 5b). The corresponding quantification of the decrease of nuclear fluorescence within the first 350 s was investigated by 2P-epifluorescence, with the above mentioned intrinsic time gap of five seconds for re-tuning the wavelength of the laser (Fig. 5c). The quantification of the 2P-fluorescence data within the first 350 s is presented with a single exponential fit, strengthening the interpretation that photobleaching is not relevant in this time window. The analysis yielded a diffusion time constant of 123 s for this experiment, in good

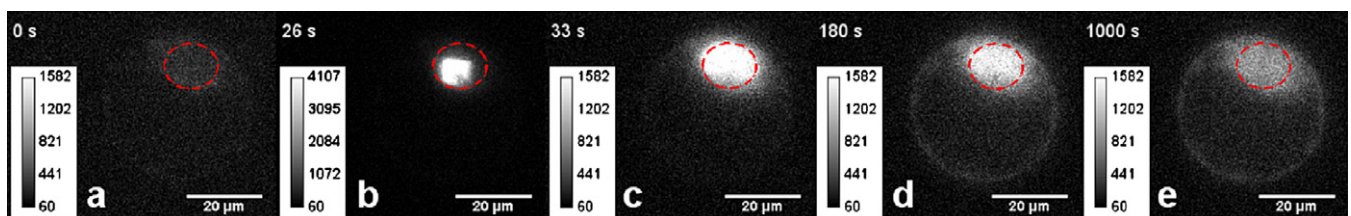


Fig. 3. Dynamics of free diffusion of pa-GFP in a live protoplast. Five selected IP-transmission fluorescence images of a tobacco BY-2 protoplast expressing pa-GFP (a) at the onset of the experiment before activation, (b) during 2P-activation of pa-GFP, and (c–e) after 2P-activation were taken at the time points indicated. (a) Before 2P-activation of pa-GFP in the nucleus (red dotted line) the average fluorescence intensity is barely detectable. 2P-activation of pa-GFP was initiated with a fs-laser burst of 3 s covering an area of  $7 \times 8 \mu\text{m}^2$  with four parallel laser foci (10 mW at 800 nm per focus). (b) Shortly after photo-activation a strong fluorescence signal was detected and (c–e) the diffusion of photo-activated pa-GFP from the nucleus into the cytoplasm was monitored until equilibrium of partitioning between the two cellular compartments was reached. Fluorescence intensity scales are shown in each panel to the left.

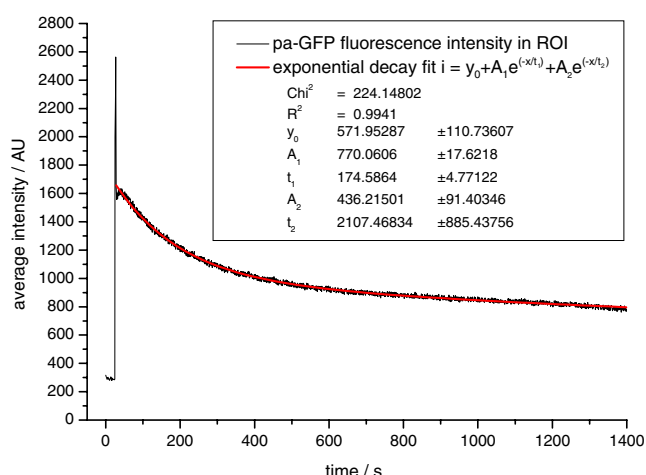


Fig. 4. Quantitative analysis of pa-GFP diffusion from the nucleus into the cytoplasm after its photo-activation in the nucleus. Before activation the averaged 1P-fluorescence intensity in the nucleus (ROI) is very low (averaged intensity  $\sim 300$ ). Between time points 26 s and 29 s the fluorescence burst induced by the fs-laser activation is monitored in the graph. Post activation, the averaged fluorescence intensity is about 5 times greater as compared to the pre-activation intensity, followed by a decrease of fluorescence in the ROI. In the first place, the monitored decrease of fluorescence intensity in the cell nucleus is due to diffusion of the activated pa-GFP into the cytoplasm. Later, also photobleaching becomes noticeable. Bi-exponential fitting describes the overall decrease of fluorescence in very good approximation (red line). In this way, a diffusion time constant of 175 s was calculated for this experiment. (For interpretation of the references to colour in this figure legend, the reader is referred to the web version of this article.)

agreement with the diffusion time constant in a similar experiment measured with 1P-fluorescence (Fig. 4).

### 3.5. Protein dynamics of the MYB transcription factor LCL1 fused to pa-GFP

In contrast to the diffusion of nuclear-activated pa-GFP through the nuclear pore complexes into the cytoplasm, the localisation dynamics of the MYB transcription factor LCL1 fused to pa-GFP depends on active nuclear export versus active nuclear import both of which are receptor-mediated (Merkle, 2003; compare Fig. 2). Protoplasts co-transfected with At2g38360-DsRed and pa-GFP-LCL1 were subjected to the 2P-activation procedure and the decrease of nuclear fluorescence intensity was monitored with 1P-fluorescence microscopy (Figs. 6a and b). Quantitative analysis of these data revealed adequate fitting with a bi-exponential function, giving two time constants of 4.7 s and 20.6 s, respectively (Fig. 6b). While the first time constant can be attributed to non-linear short term photoactivation of DsRed (Marchant et al., 2001) the time constant of 20.6 s reflects the net translocation of pa-GFP-LCL1 out of the nucleus into the cytoplasm that finally results in the steady state localisation observed for GFP-LCL1 (Fig. 2a). This time constant is considerably smaller than that of the diffusion of pa-GFP out of the nucleus (compare Figs. 4 and 5). This result is further supported by the two-colour

2PLSM 3D voxel representation of At2g38360-DsRed and pa-GFP-LCL1, which were taken just before activation of pa-GFP (Fig. 6c) and after monitoring of the fluorescence dynamics 45 s after starting the complete measurement cycle (Fig. 6d).

### 3.6. Protein dynamics of the export-negative mutant pa-GFP-LCL1(NESm)

As a control experiment, an export-negative mutant version of LCL1 (compare Figs. 2e, f) was fused to pa-GFP and its dynamics after 2P-activation in the nucleus was quantitatively analysed in the same way. In Fig. 7a a typical experiment with a protoplast expressing At2g38360-DsRed and pa-GFP-LCL1(NESm) after 2P-activation of pa-GFP in the nucleus and quantitative analysis of protein dynamics using 1P-fluorescence is shown. After the activation burst, the average activated fluorescence intensity in the ROI remains almost constant. The only significant decrease of nuclear fluorescence that was detected over a time period of nearly 6 min was due to photobleaching of pa-GFP. Therefore, no exponential fit could be applied to the data, since putative nuclear fluorescence decrease time constants were significantly larger than the duration of the experiment. Migration of the activated pa-GFP-LCL1(NESm) out of the nucleus into the cytoplasm was not observed. This is also reflected by the corresponding two-colour 2PLSM 3D voxel representation (Figs. 7b and c) that were taken just before (Fig. 7b) and after monitoring the fluorescence decrease over time (Fig. 7c).

## 4. Discussion

The development of a photo-activatable variant of GFP (Patterson and Lippincott-Schwartz, 2002) created a powerful tool for real-time measurement of protein dynamics in living cells. Especially, well-defined local photo-activation of pa-GFP fusion proteins within the cell is of crucial importance for addressing relevant sub-populations of these fusion proteins. This can only be accomplished by 2P excitation. For this reason, we combined the analysis of the localisation and dynamics of pa-GFP fusion proteins with 2PLSM that offered both locally confined photo-activation and specific 3D detection of photo-activated fluorophores.

Using tobacco BY-2 protoplasts transfected with pa-GFP driven by a strong constitutive promoter, we showed that this approach offers a fast access to real-time measurement of protein dynamics (Figs. 3–5). First, we showed that 2P-activation of pa-GFP in the nucleus using multifocal femtosecond laser pulses worked very efficiently (Figs. 3 and 4). Second, after 2P-activation of pa-GFP, the re-distribution of pa-GFP from the nucleus into the cytoplasm could be easily recorded by either 2PLSM at 920 nm (Fig. 5) or by conventional 1P-fluorescence microscopy (Fig. 3). Third, by defining a ROI at the site of 2P-activation in the nucleus, quantitative measurement of pa-GFP re-distribution was possible. We showed that the decrease

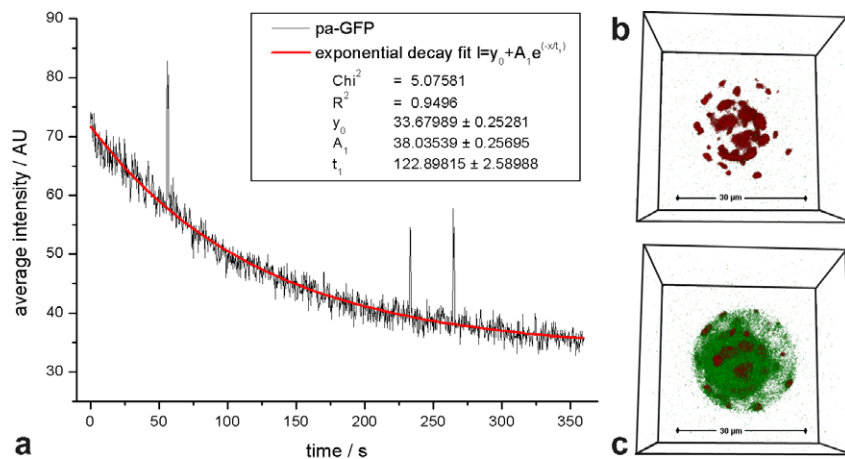


Fig. 5. Localisation of At2g38360-DsRed and 3D monitoring of pa-GFP dynamics by parallel 2P-epifluorescence microscopy (64 foci, 920 nm, 240 mW) in a tobacco BY-2 protoplast. (a) Quantitative analysis of the decrease of nuclear pa-GFP 2P-epifluorescence, giving a diffusion time constant of 123 s. The data shown in Figs. 3 and 4 emanate from two different experiments, explaining the difference in absolute numbers for fluorescence values (different expression levels) and statistical analysis. (b) Fluorescence of At2g38360-DsRed as a transfection marker before activation of pa-GFP in the nucleus, and (c) 3D fluorescence image of At2g38360-DsRed and pa-GFP 400 s after data sampling, clearly demonstrating the diffusion of fluorophores from the nucleus into the cytoplasm.

of fluorescence in the nuclear ROI could be described very accurately either by mono- or bi-exponential function. Forth, using parallel 2PLSM at 920 nm, 3D analysis of protein dynamics before and after photo-activation was monitored (Figs. 5–7).

pa-GFP does not contain any localisation signals and constitutes a small soluble protein of about 27 kDa. The

distribution of pa-GFP within the protoplast after localised 2P-activation thus depends solely upon diffusion. For pa-GFP we included only those data in the calculation of the average time constant that showed a correlation of  $R^2 > 0.94$  in the statistical analysis. As a result, pa-GFP showed diffusion from the nucleus to the cytoplasm after photo-activation in the nucleus with an average time

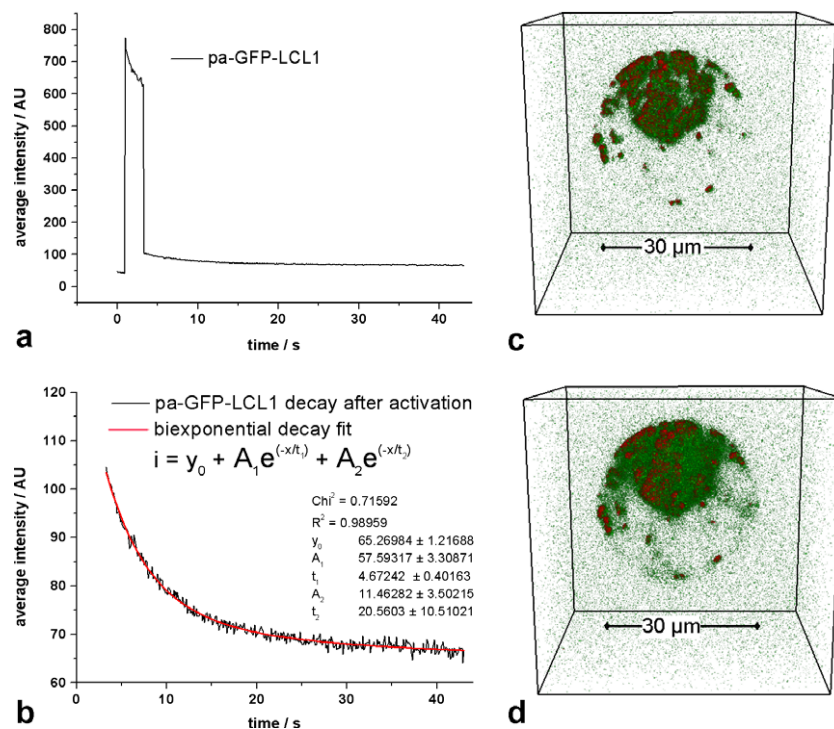


Fig. 6. Quantitative analysis and 3D monitoring of the dynamics of actively translocated pa-GFP-LCL1 before and after its photo-activation in the nucleus in a tobacco BY-2 protoplast. (a) 1P-fluorescence in the nucleus after 2P-activation of pa-GFP-LCL1 showing the 2P-activation fluorescence burst. (b) Quantitative analysis of the post-activation decrease of pa-GFP in the nucleus by 2P-epifluorescence with a bi-exponential fit (red line). A time constant of 20 s was calculated for the nuclear fluorescence decrease of pa-GFP-LCL1 due to active transport. (c,d) Two-colour-2P-epifluorescence 3D maps of At2g38360-DsRed (transfection marker) and pa-GFP-LCL1 taken (c) just before photo-activation of pa-GFP in the nucleus and (d) after data sampling.

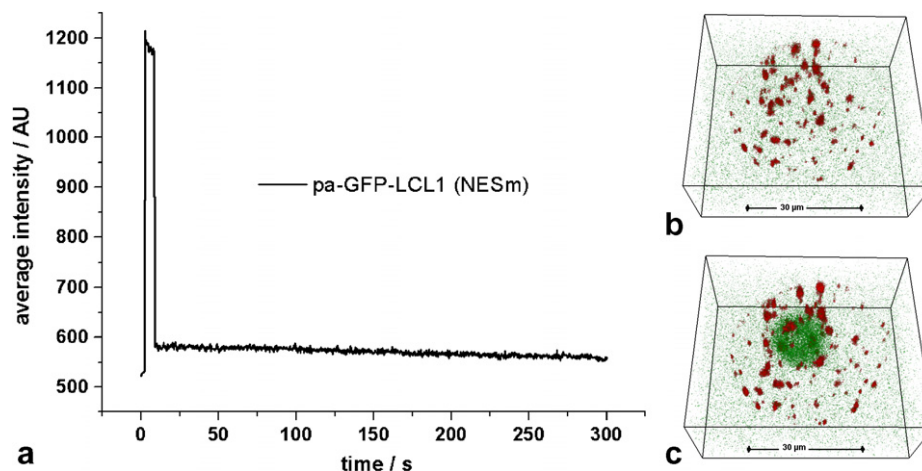


Fig. 7. Quantitative analysis and 3D monitoring of the dynamics of the nuclear export-negative mutant pa-GFP-LCL1(NESm) before and after its photo-activation in the nucleus in a tobacco BY-2 protoplast. (a) 1P-fluorescence in the nucleus after 2P-activation of pa-GFP-LCL1(NESm) showing the 2P-activation fluorescence burst and an extremely slow decrease of nuclear fluorescence post-activation, reflecting the nuclear trapping of pa-GFP-LCL1(NESm). (b,c) Two-colour 2P-epifluorescence 3D maps of At2g38360-DsRed (transfection marker) and pa-GFP-LCL1(NESm) taken (b) just before photo-activation of pa-GFP in the nucleus and (c) after data sampling at time point 300 s.

constant of  $125.06 \pm 33.15$  s. This has been measured on a statistical base of 7 cells and compares very well with a decay time constant of 200 s as published by Chen et al. (2006).

However, we applied this novel combination of methods to fast biological processes that are highly relevant for regulation, such as nuclear export of transcription factors as a fast and reversible means to regulate gene expression (Merkle, 2003). We have characterised the nuclear export receptor Exportin 1 (Arabidopsis XPO1, in humans called CRM1) and have shown that nuclear export processes in plants are sensitive to the cytotoxin leptomycin B (LMB; (Haasen et al., 1999); see Figs. 2a–d). The transcription factor LCL1 contains both a classic basic monopartite NLS that links it to the nuclear import machinery via Importin  $\alpha/\beta$  heterodimers, and an NES that confers interaction with XPO1 (Merkle, 2003; Schmied and Merkle, submitted for publication). The equilibrium localisation of LCL1 that is detected with GFP-LCL1 in protoplasts by IPLSM (Fig. 2a) is thus a balance between active nuclear export and re-import. This could be demonstrated indirectly by inhibiting nuclear export processes by LMB, resulting in a shift of the equilibrium localisation of GFP-LCL1 (nucleus and cytoplasm) towards an almost nuclear localisation in the presence of LMB (Fig. 2b). In this work, we directly show the dynamics that underlie the equilibrium localisation of this shuttling transcription factor. We detected a very fast decrease of fluorescence in the nuclear ROI after photo-activation of pa-GFP-LCL1 in the nucleus (Figs. 6a and b). Since nuclear export and import are very fast processes (Ribbeck and Gorlich, 2001), we expected a very rapid decrease of fluorescence during and immediately after photo-activation, which we did (Fig. 6a). 3D 2PLSM maps of pa-GFP-LCL1 before and after photo-activation (45 s after start of recording) show that equilibrium between the nucleus and the cytoplasm was reached much faster than

with pa-GFP alone (Figs. 6c and d). For pa-GFP-LCL1 we used only fluorescence decay data which could be fitted with  $R^2 > 0.95$  to mono- or bi-exponential decays. Based on a statistics of seven individually measured cells, the average time constant for nucleo-cytoplasmic partitioning of pa-GFP-LCL1 after photo-activation in the nucleus is  $50.97 \text{ s} \pm 38.5$  s.

In contrast to pa-GFP-LCL1, statistical analysis of the dynamics of the export-negative variant pa-GFP-LCL1(NESm) that does not interact any more with the export receptor XPO1 (Merkle, 2003; Schmied and Merkle, submitted for publication) revealed that there was only a very slow decrease in average fluorescence intensity inside the nuclear ROI after photo-activation in the nucleus (Fig. 7), which most probably was due to bleaching of activated fluorophores, only. We concluded that except for a very fast distribution within the nucleus, there was no detectable protein dynamics. pa-GFP-LCL1(NESm) is devoid of a functional NES but still contains a functional NLS and accumulates in the nucleus (compare Figs. 2e and f). Therefore, average time constants were not determined in this case, especially as they would have required observation periods of much more than 1000 s.

It is worth noting that during transfection the number of plasmids entering the protoplasts cannot be controlled. Due to this reason, quite different expression levels are observed, explaining the variation in absolute fluorescence values and statistical analysis.

In summary, we presented a new methodological approach and application for quantitatively monitoring dynamic processes *in vivo* by a combination of localised and selective fluorescence activation by two-photon excitation in combination with quantitative real-time fluorescence one/two photon microscopy. We were able to monitor *in vivo* the intracellular dynamics of the Arabidopsis MYB transcription factor LHY/CCA1-like 1 (LCL1)

from the nucleus into the cytoplasm. This method and its application demonstrate, that dynamic cellular processes can be investigated and analyzed *in vivo* by novel biophysical microscopy methods opening new possibilities towards a more quantitative biology.

### Acknowledgments

This work was supported by the research project MEMO (13N8432) within the research framework BIOPHOTONICS I from the Federal Ministry of Education and Research of Germany (BMBF) to D.A. In addition, T.M. and R.P. acknowledge financial support by the DFG (BIZ 7/1-2, ME 1116/4-2, PA1479/1-1). We are grateful to Bernd Weisshaar for his generous support and thank Ute Buerstenbinder and Christoph Pelargus for excellent technical assistance.

### References

- Albota, A.A., Xu, C., Webb, W.W., 1998. Two-photon fluorescence excitation cross sections of biomolecular probes from 690 to 960 nm. *Applied Optics* 37, 7352–7356.
- Cahalan, M.D., Parker, I., Wei, S.H., Miller, M.J., 2002. Two-photon tissue imaging: seeing the immune system in a fresh light. *Nature* 2, 872–880.
- Chen, Y., MacDonald, P.J., Skinner, J.P., Patterson, G.H., Muller, J.D., 2006. Probing nucleocytoplasmic transport by two-photon activation of PA-GFP. *Microsc. Res. Tech.* 69, 220–226.
- Denk, W., Strickler, J.H., Webb, W.W., 1990. Two-photon laser scanning fluorescence microscopy. *Science* 248, 73–76.
- Diaspro, A., 2002. *Confocal and Two-Photon Microscopy: Foundations, Applications, and Advances*, Wiley-Liss, Inc., New York.
- Fornierod, M., Ohno, M., Yoshida, M., Mattaj, I.W., 1997. CRM1 is an export receptor for leucine-rich nuclear export signals. *Cell* 90, 1051–1060.
- Fukuda, M., Asano, S., Nakamura, T., Adachi, M., Yoshida, M., Yanagida, M., Nishida, E., 1997. CRM1 is responsible for intracellular transport mediated by the nuclear export signal. *Nature* 390, 308–311.
- Haasen, D., Kohler, C., Neuhaus, G., Merkle, T., 1999. Nuclear export of proteins in plants: AtXPO1 is the export receptor for leucine-rich nuclear export signals in *Arabidopsis thaliana*. *Plant J.* 20, 695–705.
- Hutt, D.M., Da Silva, L.F., Chang, L.H., Prosser, D.C., Ngsee, J.K., 2000. PRA1 inhibits the extraction of membrane-bound rab GTPase by GDI1. *J. Biol. Chem.* 275, 18511–18519.
- König, K., 2000. Multiphoton microscopy in life sciences. *J. Microsc.* 200, 83–104.
- Kudo, N., Matsumori, N., Taoka, H., Fujiwara, D., Schreiner, E.P., Wolff, B., Yoshida, M., Horinouchi, S., 1999. Leptomycin B inactivates CRM1/exportin 1 by covalent modification at a cysteine residue in the central conserved region. *Proc. Natl. Acad. Sci. USA* 96, 9112–9117.
- Marchant, J.S., Stutzmann, G.E., Leissring, M.A., LaFerla, F.M., Parker, I., 2001. Multiphoton-evoked color change of DsRed as an optical high-lighter for cellular and subcellular labeling. *Nat. Biotechnol.* 19, 645–649.
- Martini, J., Tönsing, K., Dickob, M., Anselmetti, D., 2005. 2-Photon laser scanning microscopy on native human cartilage. In: Wilson, T. (Ed.), *Proceedings of SPIE [Confocal, Multiphoton, and Nonlinear Microscopic Imaging II]*, vol. 5860, pp. 16–21.
- Martini, J., Tönsing, K., Dickob, M., Schade, R., Liefelth, K., Anselmetti, D., 2006. 2-Photon laser scanning microscopy on native human cartilage and collagen-membranes for tissue engineering. *Proceedings of SPIE*, vol. 6089, pp.274–282.
- Merkle, T., 2003. Nucleo-cytoplasmic partitioning of proteins in plants: implications for the regulation of environmental and developmental signalling. *Curr. Genet.* 44, 231–260.
- Nielsen, T., Fricke, M., Hellweg, D., Andresen, P., 2001. High efficiency beam splitter for multifocal multiphoton microscopy. *Journal of Microscopy* 201, 368–376.
- Patterson, G.H., Lippincott-Schwartz, J., 2002. A photoactivatable GFP for selective photolabeling of proteins and cells. *Science* 291, 1873–1877.
- Patterson, G.H., Lippincott-Schwartz, J., 2004. Selective photolabeling of proteins using photoactivatable GFP. *Methods* 32, 445–450.
- Post, J.N., Lidke, K.A., Rieger, B., Arndt-Jovin, D.J., 2005. One- and two-photon photoactivation of a paGFP-fusion protein in live *Drosophila* embryos. *FEBS Lett.* 579, 325–330.
- Rasband, W.S. ImageJ. [1997–2005] 1997. <http://rsb.info.nih.gov/ij/>, U.S. National Institutes of Health, Bethesda, MD, USA.
- Ribbeck, K., Gorlich, D., 2001. Kinetic analysis of translocation through nuclear pore complexes. *EMBO J.* 20, 1320–1330.
- Schaffer, R., Ramsay, N., Samach, A., Corden, S., Putterill, J., Carre, I.A., Coupland, G., 1998. The late elongated hypocotyl mutation of *Arabidopsis* disrupts circadian rhythms and the photoperiodic control of flowering. *Cell* 93, 1219–1229.
- Schmied, K., Merkle, T., submitted for publication. The *Arabidopsis* LHY/CCA1-like (LCL) protein family: MYB transcription factors containing a nuclear export signal are co-regulators of the circadian clock.
- Schneider, M., Barozzi, S., Testa, I., Faretta, M., Diaspro, A., 2005. Two-photon activation and excitation properties of PA-GFP in the 720–920-nm region. *Biophys. J.* 89, 1346–1352.
- Wang, Z.Y., Tobin, E.M., 1998. Constitutive expression of the circadian clock associated 1 (CCA1) gene disrupts circadian rhythms and suppresses its own expression. *Cell* 93, 1207–1217.
- Zipfel, W.R., Williams, R.M., Christie, R., Nikitin, A.Y., Hyman, B.T., Webb, W.W., 2003a. Live tissue intrinsic emission microscopy using multiphoton-excited native fluorescence and second harmonic generation. *Proc Natl. Acad. Sci. USA* 100, 7075–7080.
- Zipfel, W.R., Williams, R.M., Webb, W.W., 2003b. Nonlinear magic: multiphoton microscopy in the biosciences. *Nat. Biotech.* 21, 1369–1377.